ROYAL SOCIETY
OF CHEMISTRY

PAPER

Check for updates

Construction of a Keggin heteropolyacid/Ni-MOF catalyst for esterification of fatty acids†

Qiuyun Zhang, [ID] *[abc] Qizhi Luo,[a] Yaping Wu,[a] Rongfei Yu,[a] Jingsong Cheng[a] and Yutao Zhang*[abc]

This work reports the one-pot solvothermal synthesis of a Keggin heteropolyacid (phosphomolybdic acid, tungstophosphoric acid, or silicotungstic acid) immobilized on Ni-MOF composite catalysts for esterification of fatty acids, and the composites were further analyzed by XRD, FTIR, NH_3-TPD, SEM, TEM, N_2 adsorption/desorption, and XPS. Among the contrastive syntheses (*i.e.*, HPW/Ni-MOF, HSiW/Ni-MOF, and HPMo/Ni-MOF), HPMo/Ni-MOF exhibits the most active catalyst toward fatty acids esterification, and the characterization results also revealed that HPMo/Ni-MOF has a strong acidity, large specific surface area, and appropriate average pore size. More significantly, this catalyst exhibits a good catalytic performance (86.1% conversion) during esterification under the optimized reaction conditions, and the HPMo/Ni-MOF catalyst can remain stable after the tenth cycle with a conversion of 73.5%. Intriguingly, the esterification reaction kinetics was studied, and the activation energy was found to be 64.6 kJ mol^{-1}. The results indicated that the esterification of fatty acids using the HPMo/Ni-MOF catalyst is a chemically controlled reaction.

1. Introduction

Over the past few decades, the rapid development of the global economy and the use of fossil fuels has resulted in many problems, such as global warming and climate change, smog, and acid rain.[1,2] Seeking more renewables to meet the sustainable development of the global economy, including biofuels, and wind and solar energy, can reduce the dependence on fossil fuels.[3] Amongst the biofuels, biodiesel, or fatty acid methyl esters, has great potential as an alternative owing to the advantages of biodegradability, low sulfur content, high combustion efficiency and flash point, as well as lowering pollutant emission.[4] Typically, biodiesel is derived from the transesterification of edible oils[5] and inedible oils (Jatropha oil,[6] waste cooking oil[7] *etc.*) or esterification of free fatty acids (FFAs)[8] with short-chain alcohols with the help of base/acid catalysts. Generally, inedible oils are more feasible as raw oils due to their reduced cost in biodiesel processing, but they contain lots of FFAs or water which cause saponification in the presence of base catalysts.[9] Then, the conversion of FFAs into

esters *via* esterification in the presence of acidic catalysts is needed for inedible oils.

In the actual production processes, liquid acid catalyst usually can get a high reaction rate and high conversion.[10] Unfortunately, the liquid acid catalytic system is suffering from separation difficulty, equipment corrosion, and production of large quantities of wastewater.[11] Compared to liquid acid catalyst, solid acid catalyst, such as heteropolyacid,[12] resins,[13] ionic liquid,[14] carbon-based solid acid catalyst,[15] *etc.*, could provide more advantages, such as eco-friendly, easy separation, great reusability and sustainability for esterification process. However, these solid acid catalysts also have some drawbacks: complex preparation process, high-cost synthesis, active component leaching, and low catalytic activity.[16]

Among solid acid catalysts, the Keggin heteropolyacid (such as phosphomolybdic acid, tungstophosphoric acid, silicotungstic acid) have been received widely considerable attention as acid catalyst owning to its strong Brønsted acidity and versatility of modifications.[17] However, heteropolyacid can be easily dissolved in polar solvents (*e.g.* water, alcohols, ketones, *etc.*) led to homogeneous catalytic, and the surface area of heteropolyacid is too low, which limited the use for catalysis.[18] One feasible way to solve above-mentioned limitations is immobilized heteropolyacid on a supporter (*e.g.* metal–organic framework (MOF),[19,20] SBA-15,[21] zeolites,[22] Al_2O_3,[23] *etc.*), and it could be easily separated from reaction system at a low cost, and it also had a large specific surface area for providing more active sites and improving the economic feasibility. Among them, MOF can be as a new class of porous carrier materials for

[a]School of Chemistry and Chemical Engineering, Anshun University, Anshun 561000, Guizhou, China. E-mail: sci_qyzhang@126.com; zyt0516@126.com

[b]College Rural Revitalization Research Center of Guizhou, Anshun, 561000, Guizhou, China

[c]Engineering Technology Center of Control and Remediation of Soil Contamination of Guizhou Science and Technology Department, Anshun University, Anshun, 561000, Guizhou, China

† Electronic supplementary information (ESI) available. See DOI: 10.1039/d1ra06023f

applications in various fields owning to its permanent porosity, high specific surface area, and diverse functionality structure.[24–27] Masoumi *et al.* had prepared the PTA/MIL-53 (Fe) composite through the encapsulation method, and it can be as a good adsorbent for tetracycline hydrochloride removal.[28] Wang *et al.* developed a composite material (HPMo@UiO-66) for oxidative desulfurization, and it exhibited excellent catalytic performance.[29]

Inspired by the above study, herein, we present a one-pot solvothermal approach to prepare a series of Keggin heteropolyacid/Ni-MOF catalysts for the direct esterification of fatty acids. These catalysts are characterized using various techniques to reveal their compositions, morphology, structures, and acidic properties. Additionally, the reaction kinetics, recyclability, and comparison studies of fatty acids esterification reactions are also examined.

2. Experimental section

2.1 Chemicals and materials

The chemicals of nickel(II) nitrate hexahydrate ($Ni(NO_3)_2 \cdot 6H_2O$, AR), phosphomolybdic acid ($H_3PMo_{12}O_{40} \cdot nH_2O$, HPMo, AR), tungstophosphoric acid ($H_3PW_{12}O_{40} \cdot nH_2O$, HPW, AR), silicotungstic acid (HSiW, $H_4SiW_{12}O_{40} \cdot nH_2O$, HSiW, AR), and terephthalic acid (H_2-BDC, AR) are purchased from Shanghai Aladdin Biochemical Technology Co., Ltd, Shanghai, China. Absolute ethanol (AR), oleic acid (C18:1, AR), anhydrous methanol (AR), and *N,N*-dimethylformamide (DMF, AR) are purchased from Sinopharm Chemical Reagent Co., Ltd, Shanghai, China. These chemicals are directly used without further purification.

2.2 Synthesis of Keggin heteropolyacid/Ni-MOF catalyst

The synthesis of a series of Keggin heteropolyacid/Ni-MOF catalysts was carried out *via* a typical solvothermal method with some modifications.[30] Firstly, 2 mmol $Ni(NO_3)_2 \cdot 6H_2O$ was dissolved into the mixture solvent consisting of 32 mL DMF, 2 mL absolute ethanol, and 2 mL distilled water, and ultrasonized at room temperature for 10 min. Secondly, 1 mmol H_2-BDC and 0.5 g Keggin heteropolyacid (HPMo, HPW, HSiW) were slowly added into above mixed solution, and the mixture solution was stirred at room temperature for another hour to obtain a green mixed solution. Then, transferred to a Teflon autoclave (50 mL), and kept in the oven at 150 °C for 6 h. Finally, the reaction mixture was cooled to room temperature and was collected by centrifugation, washed with DMF and distilled water three times, and dried at 90 °C for 12 h under vacuum to gain the Keggin heteropolyacid/Ni-MOF catalyst and named as HPMo/Ni-MOF, HPW/Ni-MOF, HSiW/Ni-MOF, respectively.

2.3 Characterization

The Fourier transform infrared (FTIR) spectra were recorded on the infrared spectrometer (PerkinElmer spectrum100). The catalysts were manifested in the test range of 5°–70° by wide-angle X-ray diffraction (XRD, D8 ADVANCE, equipped with CuKͺ (1.5406 Å) radiation). The morphological images of the
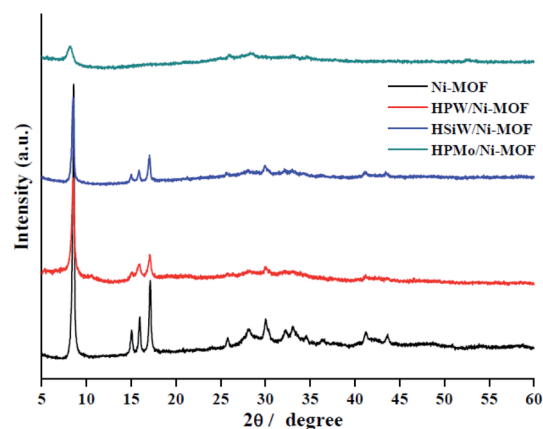

Fig. 1 XRD patterns of the Ni-MOF, HPMo/Ni-MOF, HPW/Ni-MOF, and HSiW/Ni-MOF composites.

catalysts were studied by the scanning electron microscope (SEM, Hitachi S4800) and transmission electron microscope (TEM, FEI Tecnai G2 20). The microstructure parameters of the catalyst were performed on the nitrogen adsorption–desorption analysis (Quantachrome Instruments). The acidic of catalyst is measured *via* temperature programmed desorption of NH_3 (NH_3-TPD, Micromeritics, AutoChem II 2920 instrument). The analysis of elements was measured by X-ray photoelectron spectroscopy (XPS, Thermo ESCALAB 250XI).

2.4 General procedure for esterification

The Keggin heteropolyacid/Ni-MOF catalyst was previously activated at 90 °C for 2 h. Then, a mixture of oleic acid (3.0 g), the proper amounts of methanol, and various amounts of Keggin heteropolyacid/Ni-MOF was taken in a 50 mL high-pressure autoclave, and then heated at 160 °C in an oil bath for the appropriate time. After the reaction, the catalyst was separated through centrifugation, and the excess methanol and water were vaporized from liquid product and analyzed *via* the acid value according to the method described in ISO 660-2009
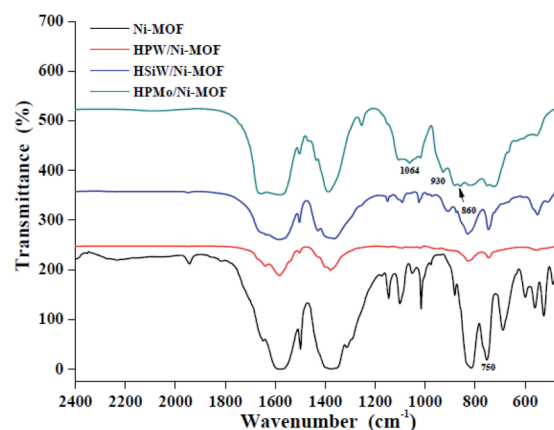

Fig. 2 FTIR spectra of the Ni-MOF, HPMo/Ni-MOF, HPW/Ni-MOF, and HSiW/Ni-MOF composites.
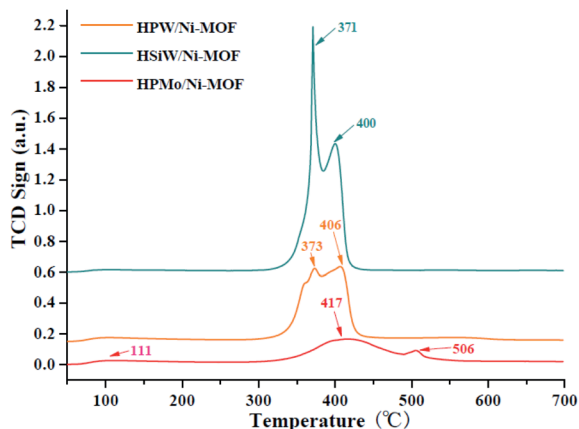
Fig. 3 TPD-NH$_3$ analysis of HPMo/Ni-MOF, HPW/Ni-MOF, and HSiW/Ni-MOF composites.

standard, and the obtain acid value before reaction and after reaction to get the conversion.

3. Results and discussion

3.1 Catalyst characterization

Fig. 1 shows the XRD figure of the Ni-MOF, HPMo/Ni-MOF, HPW/Ni-MOF, and HSiW/Ni-MOF composites. The pure Ni-MOF appears typical diffraction peaks at 8.3°, 15.0°, 15.9°, 17.0°, 25.8°, 28.1°, and 30.0° are corresponding to literature reports.[31] For HPW/Ni-MOF, and HSiW/Ni-MOF composites, the diffraction peaks perfectly match with the patterns of Ni-MOF, but the main peak intensities decreased, confirming that the structure of the Ni-MOF matrix almost kept intact after

introduction of heteropolyacid.[32] Surprisingly, for HPMo/Ni-MOF, the main diffraction peaks of Ni-MOF are partly disappeared, but it can still observe characteristic peaks at 8.1°, 25.8°, and 28.3°, this result could be interpreted as the interaction between HPMo and Ni-MOF. In addition, it also reveals that the existence of HPMo and Ni-MOF in the HPW/Ni-MOF composites, which will be further showed by the following FTIR, SEM, N$_2$ gas adsorption–desorption isotherms, and XPS observations.

The FTIR spectra of Ni-MOF, HPMo/Ni-MOF, HPW/Ni-MOF, and HSiW/Ni-MOF composites were recorded in the range 400–4000 cm^{-1} as presented in Fig. 2. The Ni-MOF spectrum of peaks at 1500–1650 cm^{-1} and 1300–1460 cm^{-1} are associated with the asymmetric and symmetric of the carboxyl groups (–COOH), respectively.[33] The peak at 1000–1200 cm^{-1} is correspond to the stretching vibration of C–O,[34] and peaks at 750 cm^{-1} are attributed to Ni–O vibration.[35] After composite heteropolyacid with Ni-MOF, HPMo/Ni-MOF, HPW/Ni-MOF, and HSiW/Ni-MOF have similar spectra to Ni-MOF, demonstrating that the Ni-MOF structure remained intact during the preparation of the composites. Notably, the peaks corresponding to HPMo/Ni-MOF at 1064 cm^{-1}, 930 cm^{-1}, and 860 cm^{-1} are associated with the Keggin structure of HPMo, but the characteristic peaks of HPMo/Ni-MOF exhibit red-shifted, this may be caused by the strong interaction between HPMo and Ni-MOF matrix. This suggests that the presence of both HPMo and Ni-MOF in the composites, which is consistent with the XRD analysis.

The surface acidity of the Keggin heteropolyacid/Ni-MOF catalysts are determined by the TPD-NH$_3$ technology, and the results are presented in Fig. 3. From Fig. 3, all of the catalysts
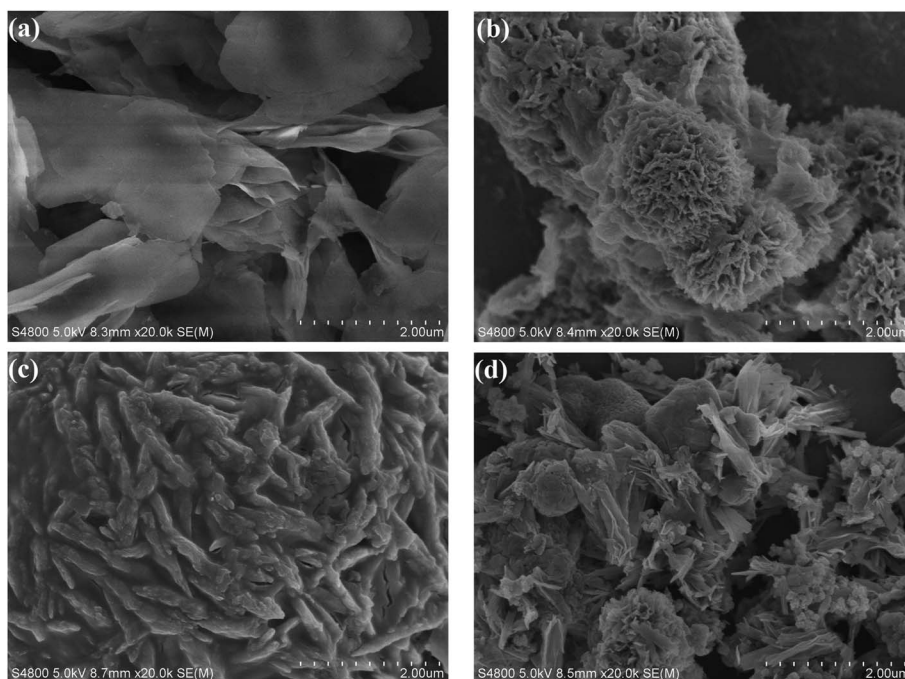

Fig. 4 SEM images of (a) Ni-MOF, (b) HPW/Ni-MOF, (c) HSiW/Ni-MOF, and (d) HPMo/Ni-MOF composites.

exhibited medium acidic properties. However, values of maximum peaks for HPMo/Ni-MOF in 417 °C are 11 °C and 17 °C higher than those of HPW/Ni-MOF and HSiW/Ni-MOF, respectively, it reveals that HPMo/Ni-MOF composite has a high acidity compare to HPW/Ni-MOF and HSiW/Ni-MOF. Also, peak at 111 °C implies the existence of weak Lewis acidic sites, which may be related to the hydroxyl groups on the surface of HPMo/Ni-MOF composite. Surprisingly, the HPMo/Ni-MOF sample displayed a maximum desorption peak at 506 °C due to the existence of strong Brønsted acidic sites with the introduction of HPMo, so it was not surprising for its excellent activity in the esterification reaction.

The morphology of Ni-MOF, HPMo/Ni-MOF, HPW/Ni-MOF, and HSiW/Ni-MOF composites were observed by SEM. In Fig. 4a, Ni-MOF powders were composed of irregularly wrinkled nanosheet structure, and the results also agree well with the previous report.[36] When heteropolyacid loaded, the morphology of the composites changed significantly. Among them, the morphology of HPW/Ni-MOF looks like flowers (Fig. 4b) and the morphology of HSiW/Ni-MOF exhibits an irregularly aggregate bar of particles (Fig. 4c). In contrast, HPMo/Ni-MOF was mainly composed of wrinkled nanosheets and flower structure (Fig. 4d), and it is possibly related to the interaction between subject and object. This analysis was consistent with the results

of XRD and FTIR. Coincidentally, some small particles with size about 50–100 nm were observed on the surface of HPMo/Ni-MOF composites, indicating that the HPMo was deposited on the Ni-MOF nanosheets. Additionally, it could be observed that the small HPMo particles were loaded onto the surface of Ni-MOF by the TEM presented in Fig. 5, and the clear hole structure was also found. Therefore, the loading of HPMo active component and unique structure can provide more active sites and high contact area for the interaction between catalysts and substrates.

To investigate the porosity of the pure Ni-MOF and HPMo/Ni-MOF, N_2 gas adsorption–desorption isotherms were performed, as shown in Fig. 6. In Fig. 6, the N_2 adsorption isotherm of pure Ni-MOF and HPMo/Ni-MOF showed a type IV characteristic curve signify the presence of mesoporous structure.[37] In addition, the BET surface areas of Ni-MOF and HPMo/Ni-MOF are measured to be 30.6 m^2 g^{-1} and 203.5 m^2 g^{-1}, the average pore diameters are 12.3 nm and 6.5 nm for Ni-MOF and HPMo/Ni-MOF. After composite HPMo with Ni-MOF, the BET surface areas appreciable increase could be related to HPMo loaded onto the Ni-MOF nanosheet, which in consistent with SEM observations and previous literature.[38] Additionally, the average pore diameters decrease is mainly caused by the introduction of HPMo occupied the surface of Ni-MOF. The above results
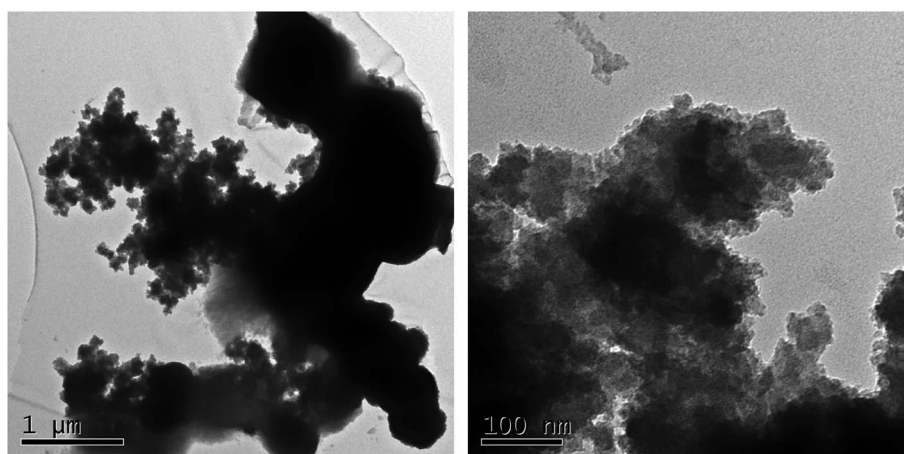

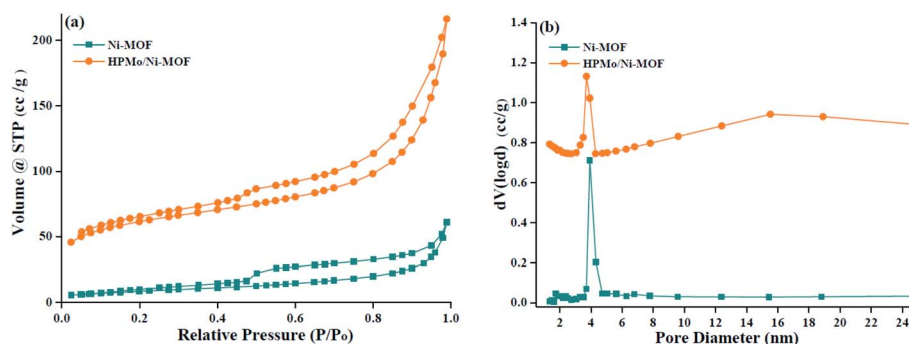Fig. 5 Typical TEM images of the HPMo/Ni-MOF composite.

Fig. 6 (a) Profiles of N_2 gas adsorption–desorption isotherms and (b) corresponding pore size distribution of Ni-MOF and HPMo/Ni-MOF composite.

demonstrate that the HPMo active guest was successfully loaded onto the surface of the Ni-MOF nanosheet. Thus, the introduction of HPMo/Ni-MOF composite may offer large BET surface areas, more catalytic sites and promote the esterification process.

XPS analysis was employed to probe the elements and surface chemical state of the HPMo/Ni-MOF composite. As demonstrated in Fig. 7a, the fully scanned spectra proved the presence of Ni, C, O, and Mo elements in HPMo/Ni-MOF. In the C 1s XPS spectra (Fig. 7b), the peaks at 284.7 eV and 288.5 eV, which can be assigned to C–C/C=C of phenyl and C=O of carboxyl, respectively.[39] Moreover, four peaks are observed at 855.6 eV, 861.5 eV are confirmed to Ni $2p_{3/2}$ and 873.5, 879.7 eV are ascribed to Ni $2p_{1/2}$, indicating the valence state of Ni is +2 (Fig. 7c).[40] Meanwhile, their satellite peaks at 861.5 eV and 879.7 eV are also found.[41] As shown in Fig. 7d, the Mo 3d XPS spectra of HPMo/Ni-MOF can be separated into two characteristic peaks at 232.5 eV and 235.6 eV, which are attributed to Mo $3d_{5/2}$ and Mo $3d_{3/2}$, respectively. Compare to previous reports,[42,43] the negative shifts of the binding energies of Mo $3d_{5/2}$ and Mo $3d_{3/2}$ of are observed, revealing the interactions exist between the Keggin unit of HPMo and Ni-MOF.[44] Hence, the XPS analysis proved the successful preparation of HPMo/Ni-MOF composites, which is consistent with the XRD, FTIR, and N_2 gas adsorption–desorption isotherms analysis.

3.2 Catalytic activity of Keggin heteropolyacid/Ni-MOF in oleic acid esterification

The obtained various Keggin heteropolyacid/Ni-MOF materials were employed as acid catalysts in the esterification of oleic acid to biodiesel. The esterification reactions were carried out at 160 °C, 0.09 g of catalyst, 1 : 20 of oleic acid to methanol molar ratio, and are as shown in Fig. 8. From Fig. 8 it can be observed that, the construction of HPW/Ni-MOF and HSiW/Ni-MOF catalysts had little catalytic activity, similar to that of pure Ni-MOF sample. To our delight, the HPMo/Ni-MOF catalyst exhibited excellent catalytic activity and the conversion of oleic acid was about 86.1%, which outperformed from the other catalyst. This may have been because of the HPMo/Ni-MOF has a high acidity, large specific surface area, and a good synergistic
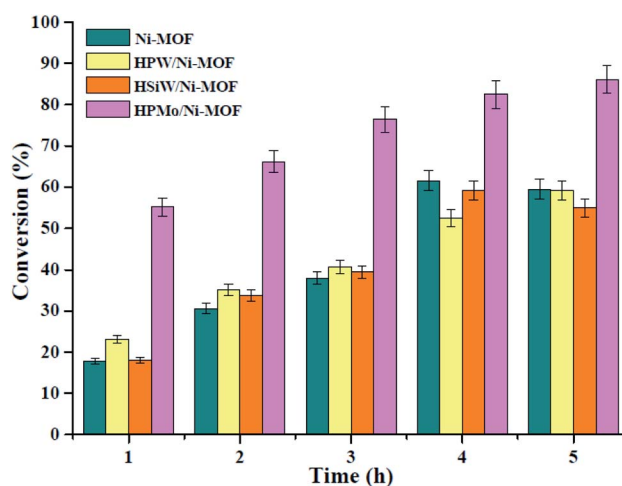

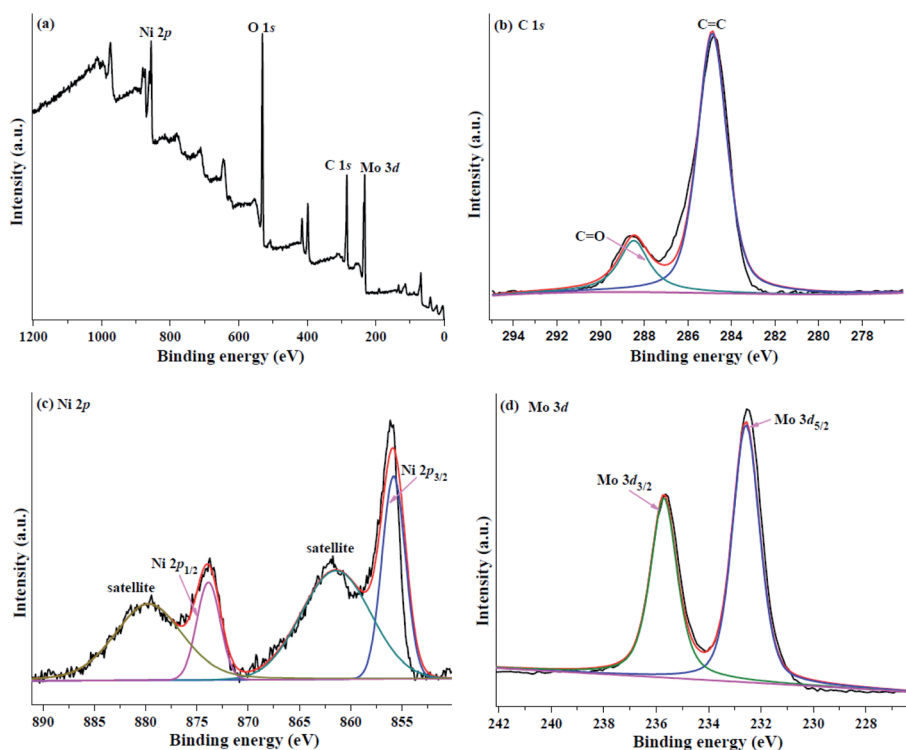Fig. 8 Reaction results of oleic acid esterification over various catalysts.

Fig. 7 XPS survey spectrum of (a) wide scan, (b) O 1s, (c) Ni 2p, and (d) Mo 3d for HPMo/Ni-MOF composite.
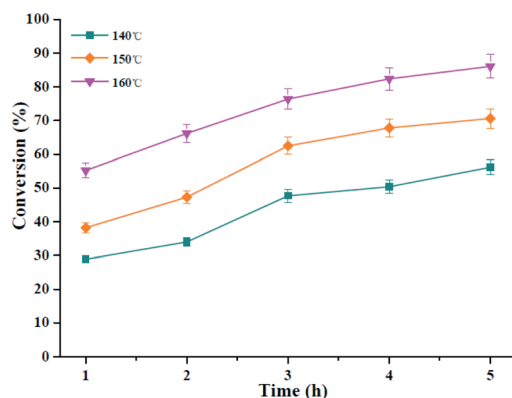
Fig. 9 Oleic acid conversion as a function of time in esterification over HPMo/Ni-MOF with different reaction temperature. Reaction conditions: 0.09 g of catalyst, 1 : 20 of oleic acid to methanol molar ratio.

effect existed between HPMo and Ni-MOF, leading to an excellent esterification activity. Then, HPMo/Ni-MOF composite was selected as target catalyst in the subsequent study.

3.3 Kinetic investigation

The kinetic behavior of the esterification process from oleic acid was studied by using HPMo/Ni-MOF composite catalyst, and the esterification experiments were performed at the reaction time range of 1–5 h and reaction temperature of 140–160 °C as shown in Fig. 9. From Fig. 9, the conversion of oleic acid increases from 50.4% to 82.4% at 4 h, as the reaction temperature increases from 140 °C to 160 °C.

According to previous literature, the rate of oleic acid esterification reaction is expected to obey the pseudo first-order reaction due to the presence of excess methanol.[45] Then, the kinetics equation as depicted following: $-\ln(1 - \eta) = kt$, and η is the conversion at time 't'. The linear relationship of $-\ln(1 - \eta)$ against time (h) was plotted at the temperatures range of 140–160 °C to study the rate constant k as drawn in Fig. 10a. From Fig. 10a, it is clear that the kinetic model gave high correlation coefficient (R^2) values above 0.9. Meanwhile, the k value increases with the increase in reaction temperature, which suggests the reaction temperature of 160 °C is optimum. Also, the activation energy of oleic acid esterification was calculated

through Arrhenius equation ($\ln k = -E_a/RT + \ln A$), and as displayed in Fig. 10b. According to this figure, the activation energy was determined as 64.6 kJ mol^{-1}, indicating that the esterification is not mass or diffusion controlled, but chemically controlled reaction.[46] Moreover, the activation energy was similar to previous literatures.[47,48]

3.4 Recycle test

To display the good recycling nature of HPMo/Ni-MOF composite, a recycle test was performed. After the reaction, catalyst was collected by centrifugation, and directly used in the next run, and the results are given in Fig. 11. It can be seen from Fig. 11 that the oleic acid conversion after the first reaction run was 82.4% and 73.5% after tenth cycle, and there was only 8.9% conversion drop in the activity of HPMo/Ni-MOF composite was observed after the reaction. These results indicate that the recycled HPMo/Ni-MOF can maintain a high conversion. To explain the excellent reusability of catalyst, FTIR spectra were used to study the structure of HPMo/Ni-MOF (Fig. S1†), and the results indicate that the FTIR spectra of fresh and used HPMo/Ni-MOF catalyst was similar, and the acid catalyst was relatively stable throughout the esterification reactions. In addition, the reduction catalytic of HPMo/Ni-MOF is probably due to the
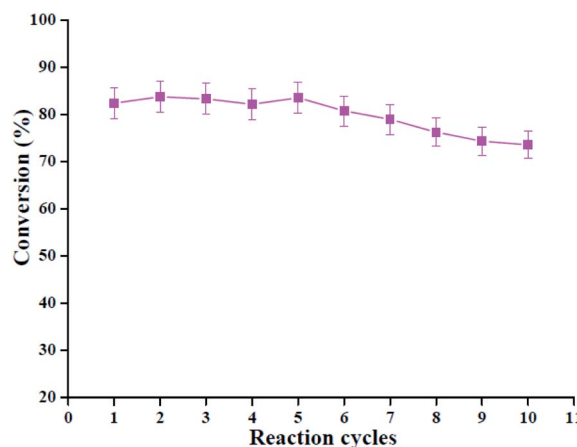

Fig. 11 Recycle performance of HPMo/Ni-MOF composite. Reaction conditions: 160 °C, 0.09 g of catalyst, 1 : 20 of oleic acid to methanol molar ratio, 4 h.
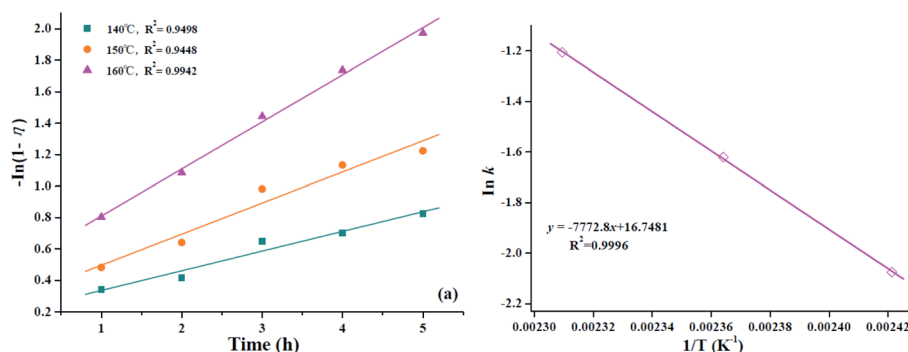

Fig. 10 (a) Plot of $-\ln(1 - \eta)$ vs. reaction time (h); (b) plot of ln k vs. 1/T (K^{-1}).

Table 1 Comparative of this study with other catalysts used in the esterification

| Catalyst | Feedstock | Catalyst (wt%) | Esterification | | | Reusability cycles | Conversion (%) | Ref. |
			M/O	Time (h)	Temp. (°C)			
WO_3/USY	Oleic acid	10	6	2	200	4	74	51
$H_3PMo_{12}O_{40}$/AC	Lauric acid	5	50	10	70	3	98	52
ZrO_2/SiO_2	Stearic acid	10	120	3	120	5	69.2	53
2.6SZA900	Oleic acid	10	5	6	70	—	71.4	54
La^{3+}-HZSM-5	Oleic acid	10	20	7	100	3	80	55
ZSM-5	Oleic acid	5	20	8	190	5	97	56
HPMo/Ni-MOF	Oleic acid	3	20	5	160	10	86.1	Current study

leaching of a small amount of HPMo and pore blockage of Ni-MOF, and a similar phenomenon has been reported for some other catalytic materials.[49,50]

3.5 Comparative study

The activity of the HPMo/Ni-MOF catalyst toward esterification has been compared with other catalysts used in the esterification of FFAs as represented in Table 1. According to Table 1, it can be concluded that the catalyst activity of HPMo/Ni-MOF in the current study has the combination of low catalyst amount and time of reaction along with excellent conversion and good reusability in comparison to other researches. Hence, the HPMo/Ni-MOF composite is an excellent catalyst for esterification with good activity, stability, and cost-effective properties.

4. Conclusion

To sum up, the Keggin heteropolyacid/Ni-MOF catalysts were successfully synthesized *via* one-pot solvothermal route and applied to esterification of oleic acid with methanol. All the composite catalysts were characterized and the catalytic activity was tested. Among them, the HPMo/Ni-MOF composite exhibits a better catalytic activity than that of HPW/Ni-MOF and HSiW/Ni-MOF, and the catalyst was found suitable up to tenth cycles with only 8.9% conversion drop. Moreover, this esterification reaction obeys first-order kinetics and the activation energy was determined as 64.6 kJ mol^{-1}. This study provides a deep insight into heteropolyacids immobilization and the composite material design for biofuels synthesis.

Funding

Conflicts of interest

There are no conflicts to declare.

References

1 I. B. Laskar, B. Changmai, R. Gupta, D. Shi, K. J. Jenkinson, A. E. H. Wheatley and L. Rokhum, A mesoporous polysulfonic acid–formaldehyde polymeric catalyst for biodiesel production from *Jatropha curcas* oil, *Renewable Energy*, 2021, **173**, 415–421.

2 H. W. Yu, Y. L. Cao, H. Y. Li, G. J. Zhao, X. Y. Zhang, S. Cheng and W. Wei, An efficient heterogeneous acid catalyst derived from waste ginger straw for biodiesel production, *Renewable Energy*, 2021, **176**, 533–542.

3 J. T. Yu, Y. H. Wang, L. Q. Sun, Z. Xu, Y. D. Du, H. L. Sun, W. Li, S. Luo, C. H. Ma and S. X. Liu, Catalysis preparation of biodiesel from waste *Schisandra chinensis* seed oil with the ionic liquid immobilized in a magnetic catalyst: Fe_3O_4@SiO_2@[C4mim]HSO_4, *ACS Omega*, 2021, **6**, 7896–7909.

4 J. Y. Chen, M. C. Li, M. T. Li, X. C. Lin and T. Qiu, Self-solidifying quaternary phosphonium-containing ionic liquids as efficient and reusable catalysts for biodiesel production, *ACS Sustainable Chem. Eng.*, 2020, **8**, 6956–6963.

5 W. L. Peng, P. Hao, J. H. Luo, B. L. Peng, X. Han and H. L. Liu, Guanidine-functionalized amphiphilic silica nanoparticles as a pickering interfacial catalyst for biodiesel production, *Ind. Eng. Chem. Res.*, 2020, **59**, 4273–4280.

6 Q. Y. Zhang, H. Li and S. Yang, Facile and low-cost synthesis of mesoporous Ti–Mo bi-metal oxide catalysts for biodiesel production from esterification of free fatty acids in *Jatropha curcas* crude oil, *J. Oleo Sci.*, 2018, **67**(5), 579–588.

7 G. H. Liu, J. Y. Yang and X. R. Xu, Synthesis of biodiesel from waste cooking oil catalyzed by b-cyclodextrin modified Mg–Al–La composite oxide, *RSC Adv.*, 2020, **10**, 26358–26363.

8 Q. Y. Zhang, D. D. Lei, Q. Z. Luo, X. J. Yang, Y. P. Wu, J. L. Wang and Y. T. Zhang, MOF-derived zirconia-supported Keggin heteropoly acid nanoporous hybrids as a reusable catalyst for methyl oleate production, *RSC Adv.*, 2021, **11**, 8117–8123.

9 Y. J. Du, L. J. Shao and C. Z. Qi, Sulfonated and cross-linked polystyrene ultrafine fibers for the esterification of palmitic acid for biodiesel production, *J. Appl. Polym. Sci.*, 2020, e50169.

10 N. Sun, M. H. Zhang, X. Q. Dong and L. T. Wang, Preparation of sulfonated ordered mesoporous carbon catalyst and its

catalytic performance for esterification of free fatty acids in waste cooking oils, *RSC Adv.*, 2019, **9**, 15941–15948.

11 S. Wang, J. L. Pu, J. Q. Wu, H. J. Liu, H. Y. Xu, X. Li and H. Wang, SO_4^{2-}/ZrO_2 as a solid acid for the esterification of palmitic acid with methanol: effects of the calcination time and recycle method, *ACS Omega*, 2020, **5**, 30139–30147.

12 W. L. Xie, C. L. Gao and H. Y. Wang, Biodiesel production from low-quality oils using heterogeneous cesium salts of vanadium-substituted polyoxometalate acid catalyst, *Catalysts*, 2020, **10**, 1060.

13 J. H. Badia, E. Ramírez, R. Soto, R. Bringúe, J. Tejero and F. Cunill, Optimization and green metrics analysis of the liquid-phase synthesis of *sec*-butyl levulinate by esterification of levulinic acid with 1-butene over ion-exchange resins, *Fuel Process. Technol.*, 2021, **220**, 106893.

14 H. Dadhania, D. Raval and A. Dadhania, Magnetically separable heteropolyanion based ionic liquid as a heterogeneous catalyst for ultrasound mediated biodiesel production through esterification of fatty acids, *Fuel*, 2021, **296**, 120673.

15 D. G. Zavarize and H. B. J. D. de Oliveira, Methanolysis of low-FFA waste cooking oil with novel carbon-based heterogeneous acid catalyst derived from Amazon açaí berry seeds, *Renewable Energy*, 2021, **171**, 621–634.

16 S. M. Ibrahim, Preparation, characterization and application of novel surface modified $ZrSnO_4$ as Sn-based TMOs catalysts for the stearic acid esterification with methanol to biodiesel, *Renewable Energy*, 2021, **173**, 151–163.

17 Q. Y. Zhang, D. Ling, D. D. Lei, J. L. Wan, X. F. Liu, Y. T. Zhang and P. H. Ma, Green and facile synthesis of metal–organic framework Cu-BTC supported Sn(II)-substituted Keggin heteropoly composites as an esterification nanocatalyst for biodiesel production, *Front. Chem.*, 2020, **8**, 129.

18 E. K. Ekinci and N. Oktar, Production of value-added chemicals from esterification of waste glycerol over MCM-41 supported catalysts, *Green Process. Synth.*, 2019, **8**, 128–134.

19 W. L. Xie, C. L. Gao and J. B. Li, Sustainable biodiesel production from low-quantity oils utilizing $H_6PV_3MoW_8O_{40}$ supported on magnetic Fe_3O_4/ZIF-8 composites, *Renewable Energy*, 2021, **168**, 927–937.

20 Q. Y. Zhang, T. T. Yang, D. D. Lei, J. L. Wang and Y. T. Zhang, Efficient production of biodiesel from esterification of lauric acid catalyzed by ammonium and silver co-doped phosphotungstic acid embedded in a zirconium metal–organic framework nanocomposite, *ACS Omega*, 2020, **5**, 12760–12767.

21 R. Tayebee, A. F. Lee, L. Frattini and S. Rostami, $H_3PW_{12}O_{40}$/SBA-15 for the solventless synthesis of 3-substituted indoles, *Catalysts*, 2019, **9**, 409.

22 Q. Han, J. Q. Ge, Y. Yang and B. J. Liu, Nickel substituted tungstophosphoric acid supported on Y-ASA composites as catalysts for the dehydration of gas-phase glycerol to acrolein, *React. Kinet., Mech. Catal.*, 2019, **127**, 331–343.

23 H. B. S. Bento, C. E. R. Reis, P. G. Cunha, A. K. F. Carvalho and H. F. De Castro, One-pot fungal biomass-to-biodiesel process: influence of the molar ratio and the concentration of acid heterogenous catalyst on reaction yield and costs, *Fuel*, 2021, **300**, 120968.

24 H. Li, M. Eddaoudi, M. O'Keeffe and O. M. Yaghi, Design and synthesis of an exceptionally stable and highly porous metal-organic framework, *Nature*, 1999, **402**, 276–279.

25 H. Dong, X. Zhang, Y. Lu, Y. Yang, Y. P. Zhang, H. L. Tang, F. M. Zhang, Z. D. Yang, X. Sun and Y. Feng, Regulation of metal ions in smart metal-cluster nodes of metal–organic frameworks with open metal sites for improved photocatalytic CO_2 reduction reaction, *Appl. Catal. A, Environ.*, 2020, **276**, 119173.

26 F. M. Zhang, L. Z. Dong, J. S. Qin, W. Guan, J. Liu, S. L. Li, M. Lu, Y. Q. Lan, Z. M. Su and H. C. Zhou, Effect of imidazole arrangements on proton-conductivity in metal–organic frameworks, *J. Am. Chem. Soc.*, 2017, **139**, 6183–6189.

27 Q. Y. Zhang, Y. T. Zhang, J. S. Cheng, H. Li and P. H. Ma, An overview of metal–organic frameworks-based acid/base catalysts for biofuel synthesis, *Curr. Org. Chem.*, 2020, **24**, 1876–1891.

28 S. Masoumi, F. F. Tabrizi and A. R. Sardarian, Efficient tetracycline hydrochloride removal by encapsulated phosphotungstic acid (PTA) in MIL-53 (Fe): Optimizing the content of PTA and recycling study, *J. Environ. Chem. Eng.*, 2020, **8**, 103601.

29 C. Wang, A. R. Li and Y. L. Ma, Phosphomolybdic acid niched in the metal-organic framework UiO-66 with defects: an efficient and stable catalyst for oxidative desulfurization, *Fuel Process. Technol.*, 2021, **212**, 106629.

30 K. Srinivas, Y. Chen, B. Wang, B. Yu, Y. Lu, Z. Su, W. Zhang and D. Yang, Metal–organic framework-derived Fe-doped $Ni_3Fe/NiFe_2O_4$ heteronanoparticle-decorated carbon nanotube network as a highly efficient and durable bifunctional electrocatalyst, *ACS Appl. Mater. Interfaces*, 2020, **12**, 55782–55794.

31 X. Han, K. Tao, Q. X. Ma and L. Han, Microwave-assisted synthesis of pillared Ni-based metal–organic framework and its derived hierarchical NiO nanoparticles for supercapacitors, *J. Mater. Sci.: Mater. Electron.*, 2018, **29**, 14697–14704.

32 D. W. Hu, X. J. Song, S. J. Wu, X. T. Yang, H. Zhang, X. Y. Chang and M. J. Jia, Solvothermal synthesis of Co-substituted phosphomolybdate acid encapsulated in the UiO-66 framework for catalytic application in olefin epoxidation, *Chin. J. Catal.*, 2021, **42**, 356–366.

33 M. H. Wang, C. B. Wang, L. Zhu, F. L. Rong, L. H. He, Y. F. Lou and Z. H. Zhang, Bimetallic NiCo metal–organic frameworks for efficient non-Pt methanol electrocatalytic oxidation, *Appl. Catal., A*, 2021, **619**, 118159.

34 A. M. Al-Enizi, M. Ubaidullah, J. Ahmed, T. Ahamad, T. Ahmad, S. F. Shaikh and M. Naushad, Synthesis of NiO_x@NPC composite for high-performance supercapacitor *via* waste PET plastic-derived Ni-MOF, *Composites, Part B*, 2020, **183**, 107655.

35 V. Ramasubbu, P. R. Kumar, E. M. Mothi, K. Karuppasamy, H. S. Kim, T. Maiyalagan and X. S. Shajan, Highly interconnected porous TiO_2–Ni-MOF composite aerogel

photoanodes for high power conversion efficiency in quasi-solid dye-sensitized solar cells, *Appl. Surf. Sci.*, 2019, **496**, 143646.

36 Y. Z. Wang, Y. X. Liu, H. Q. Wang, W. Liu, Y. Li, J. F. Zhang, H. Hou and J. L. Yang, Ultrathin NiCo-MOF nanosheets for high-performance supercapacitor electrodes, *ACS Appl. Energy Mater.*, 2019, **2**, 2063–2071.

37 Y. L. Ning, S. L. Niu, Y. Z. Wang, J. L. Zhao and C. M. Lu, Sono-modified halloysite nanotube with $NaAlO_2$ as novel heterogeneous catalyst for biodiesel production: optimization *via* GA_BP neural network, *Renewable Energy*, 2021, **175**, 391–404.

38 L. Q. Ling, Y. Tu, X. Y. Long, Q. W. Li, J. B. Gu, N. Liu and Z. Q. Li, The one-step synthesis of multiphase SnS_2 modified by NH_2-MIL-125(Ti) with effective photocatalytic performance for rhodamine B under visible light, *Opt. Mater.*, 2021, **111**, 110564.

39 P. F. Hu, C. C. Chen, Y. F. Wang, L. Pan and C. H. Lu, Room-temperature self-assembled preparation of porous $ZnFe_2O_4$/MIL-100(Fe) nanocomposites and their visible-light derived photocatalytic properties, *ChemistrySelect*, 2019, **4**, 9703–9709.

40 L. H. Yu, W. Q. Fan, N. He, Y. C. Liu, X. Han, F. Y. Qin, J. R. Ding, G. X. Zhu, H. Y. Bai and W. D. Shi, Effect of unsaturated coordination on photoelectrochemical properties of Ni-MOF/TiO_2 photoanode for water splitting, *Int. J. Hydrogen Energy*, 2021, **46**, 17741–17750.

41 M. H. Wang, C. B. Wang, L. Zhu, F. L. Rong, L. H. He, Y. F. Lou and Z. H. Zhang, Bimetallic NiCo metal–organic frameworks for efficient non-Pt methanol electrocatalytic oxidation, *Appl. Catal., A*, 2021, **619**, 118159.

42 X. Zheng, C. L. Gong, H. Liu, G. J. Wang, F. Cheng, G. W. Zheng, S. Wen and C. X. Xiong, Preparation of phosphomolybdic acid coated carbon nanotubes and its supercapacitive properties, *J. Inorg. Mater.*, 2017, **32**(2), 127–134.

43 C. Wang, A. R. Li and Y. L. Ma, Phosphomolybdic acid niched in the metal-organic framework UiO-66 with defects: an efficient and stable catalyst for oxidative desulfurization, *Fuel Process. Technol.*, 2021, **212**, 106629.

44 J. Q. Meng, X. Y. Wang, X. Yang, A. Hu, Y. H. Guo and Y. X. Yang, Enhanced gas-phase photocatalytic removal of aromatics over direct Z-scheme-dictated $H_3PW_{12}O_{40}$/g-C_3N_4 film-coated optical fibers, *Appl. Catal., B*, 2019, **251**, 168–180.

45 Z. T. Alismaeel, A. S. Abbas, T. M. Albayati and A. M. Doyle, Biodiesel from batch and continuous oleic acid esterification using zeolite catalysts, *Fuel*, 2018, **234**, 170–176.

46 M. M. Mohamed and H. El-Faramawy, An innovative nanocatalyst α-Fe_2O_3/AlOOH processed from gibbsite

47 H. R. Mahmoud, S. A. El-Molla and M. M. Ibrahim, Biodiesel production *via* stearic acid esterification over mesoporous ZrO_2/SiO_2 catalysts synthesized by surfactant-assisted sol–gel autocombustion route, *Renewable Energy*, 2020, **160**, 42–51.

48 W. Liu, P. Yin, X. Liu, S. Zhang and R. Qu, Biodiesel production from the esterification of fatty acid over organophosphonic acid, *J. Ind. Eng. Chem.*, 2015, **21**, 893–899.

49 M. H. Nazir, M. Ayoub, I. Zahid, R. B. Shamsuddin, S. Yusup, M. Ameen and M. U. Q. Zulqarnain, Development of lignin based heterogeneous solid acid catalyst derived from sugarcane bagasse for microwave assisted-transesterification of waste cooking oil, *Biomass Bioenergy*, 2021, **146**, 105978.

50 S. K. Suryajaya, Y. R. Mulyono, S. P. Santoso, M. Yuliana, A. Kurniawan, A. Ayucitra, Y. Sun, S. B. Hartono, F. E. Soetaredjo and S. Ismadji, Iron (II) impregnated double-shelled hollow mesoporous silica as acid–base bifunctional catalyst for the conversion of low-quality oil to methyl esters, *Renewable Energy*, 2021, **169**, 1166–1174.

51 A. A. Costa, P. R. S. Braga, J. L. de Macedo, J. A. Dias and S. C. L. Dias, Structural effects of WO_3 incorporation on USY zeolite and application to free fatty acids esterification, *Microporous Mesoporous Mater.*, 2012, **147**, 142–148.

52 R. G. Prado, M. L. Bianchi, E. G. da Mota, S. S. Brum, J. H. Lopes and M. J. da Silva, $H_3PMo_{12}O_{40}$/agroindustry waste activated carbon-catalyzed esterification of lauric acid with methanol: a renewable catalytic support, *Waste Biomass Valorization*, 2018, **9**(4), 669–679.

53 H. R. Mahmoud, S. A. El-Molla and M. M. Ibrahim, Biodiesel production *via* stearic acid esterification over mesoporous ZrO_2/SiO_2 catalysts synthesized by surfactant-assisted sol–gel autocombustion route, *Renewable Energy*, 2020, **160**, 42–51.

54 L. H. Tamborini, M. E. Casco, M. P. Militello, J. Silvestre-Albero, C. A. Barbero and D. F. Acevedo, Sulfonated porous carbon catalysts for biodiesel production: clear effect of the carbon particle size on the catalyst synthesis and properties, *Fuel Process. Technol.*, 2016, **149**, 209–217.

55 S. S. Vieira, Z. M. Magriotis, N. A. V Santos, A. A. Saczk, C. E. Hori and P. A. Arroyo, Biodiesel production by free fatty acid esterification using lanthanum (La^{3+}) and HZSM-5 based catalysts, *Bioresour. Technol.*, 2013, **133**, 248–255.

56 S. Mohebbi, M. Rostamizadeh and D. Kahforoushan, Efficient sulfated high silica ZSM-5 nanocatalyst for esterification of oleic acid with methanol, *Microporous Mesoporous Mater.*, 2020, **294**, 109845.